SCIENTIFIC REPORTS

OPEN

SUBJECT AREAS:
METAMATERIALS
MAGNETO-OPTICS
MAGNETIC PROPERTIES AND MATERIALS
APPLIED PHYSICS

Received
2 October 2013

Accepted
29 January 2014

Published
20 February 2014

Correspondence and requests for materials should be addressed to J.Z. (zhouji@mail.tsinghua.edu.cn)

Negative and near zero refraction metamaterials based on permanent magnetic ferrites

Ke Bi[1], Yunsheng Guo[1], Ji Zhou[1], Guoyan Dong[2], Hongjie Zhao[3], Qian Zhao[4], Zongqi Xiao[4], Xiaoming Liu[1] & Chuwen Lan[1]

[1]State Key Laboratory of New Ceramics and Fine Processing, School of Materials Science and Engineering, Tsinghua University, Beijing 100084, China, [2]College of Materials Science and Opto-Electronic Technology, University of Chinese Academy of Sciences, Beijing 100049, China, [3]Aerospace Research Institute of Special Materials and Processing Technology, Beijing 100074, China, [4]Department of Precision Instrument, School of Mechanical Engineering, Tsinghua University, Beijing 100084, China.

Ferrite metamaterials based on the negative permeability of ferromagnetic resonance in ferrites are of great interest. However, such metamaterials face a limitation that the ferromagnetic resonance can only take place while an external magnetic field applied. Here, we demonstrate a metamaterial based on permanent magnetic ferrite which exhibits not only negative refraction but also near zero refraction without applied magnetic field. The wedge-shaped and slab-shaped structures of permanent magnetic ferrite-based metamaterials were prepared and the refraction properties were measured in a near-field scanning system. The negative and near zero refractive behaviors are confirmed by the measured spatial electric field maps. This work offers new opportunities for the development of ferrite-based metamaterials.

Negative refractive index (NRI) metamaterials with simultaneously negative permittivity and negative permeability have been recently stimulated tremendous fundamental and practical interests due to their unique electromagnetic properties such as the reversals of both Doppler shift and Cherenkov radiation, enhancement of evanescent wave, and subwavelength resolution imaging, etc[1–5]. Metamaterials are a class of materials in which subwavelength features, rather than the constituent materials, control the macroscopic electromagnetic properties. Most of the reports demonstrated the metamaterials realized by periodic artificial metallic structures[6–13]. For instance, using periodic continuous wires to produce effective negative permittivity and using periodic split-ring resonators (SRRs) to provide effective negative permeability[14]. The unusual electromagnetic properties of metamaterials originate from the structure rather than being inherited directly from the materials[15], which sets great challenges for realizing the tunable and two-dimensional negative refractive properties[16,17].

Ferrite-based metamaterials have been reported in which negative magnetic permeability is achieved by substituting SRR elements with ferrites[18–23]. The negative permeability appears when the ferromagnetic resonance (FMR) of the ferrite taking place. By combining the ferrites and metallic wires, the NRI properties can be realized. In previous studies, our group designed a magnetically tunable and two-dimensional NRI metamaterial consisting of an array of yttrium iron garnet (YIG) rods and copper wires[24,25]. As the ferrites used in these metamaterials are soft magnetic materials, in order to realize the FMR and negative permeability, an external magnetic field must be applied around the ferrites, which makes the ferrite-based metamaterials difficult for practical application[20,26,27]. Recently, Harris et al.[28] outlined the advances in ferrite-based metamaterials and discussed the application of permanent magnetic ferrite in microwave devices. Gu et al.[29] designed a photonic crystal composed of self-biased strontium ferrite rods and experimentally proved that this photonic crystal can realize the negative refraction without applied magnetic field.

Here, we report a metamaterial composed of permanent magnetic ferrite rods and metallic wires, which exhibits not only negative refraction but also near zero refraction. Since no external magnetic field is needed, the near-field scanning maps can be measured with the wedge-shaped and slab-shaped samples to prove the negative and near zero refractive properties.

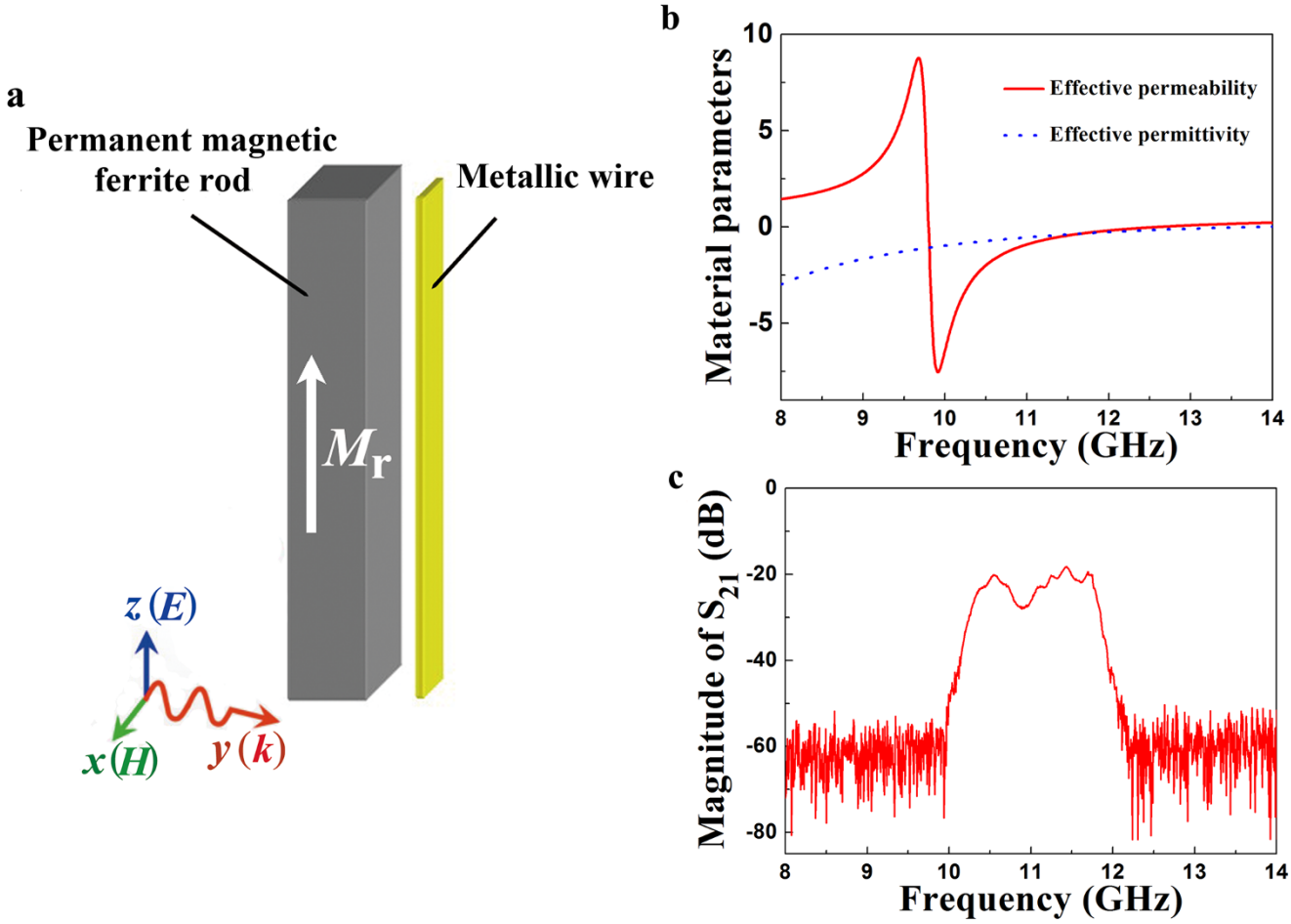

Figure 1 | Sample characterization. (a) Schematic diagram of the unit cell of one permanent magnetic ferrite rod and one metallic wire. The length directions of the permanent magnetic ferrite rod and metallic wire are parallel to the *z* axis. The propagation of the incident electromagnetic wave is along the *y* axis, and the electric field and magnetic field are along *z* and *x* directions, respectively. (b) Effective permeability and permittivity retrieved from measured scattering parameters. (c) Measured transmission spectra for permanent magnetic ferrite-based metamaterial.

Results

Theoretical calculations. The permanent magnetic ferrite-based metamaterial studied here consists of permanent magnetic ferrite rods and metallic wires. Figure 1a shows the schematic diagram of the unit cell of one permanent magnetic ferrite rod and one metallic wire. The permanent magnetic ferrite rods are used to produce effective negative permeability while the metallic wires are used to provide effective negative permittivity. With the rectangular sample of the ferrite-based metamaterials inserted into the rectangular waveguide, the scattering parameters are measured by the vector network analyzer (Agilent ENA5071C). The measured scattering parameters are used to retrieve the effective material parameters. The retrieval method is described in detail elsewhere[30]. The retrieved effective permeability μ_{eff} and effective permittivity ε_{eff} are shown in Fig. 1b. Firstly, there is one remarkable frequency dispersion in the range of 8–14 GHz and the negative μ_{eff} appears at 9.8–12.5 GHz. As the frequency increases from 9.8 GHz, one observes a decrease in μ_{eff} to a minimum. With further increase in frequency, μ_{eff} increases to a near-zero value. Secondly, it can be seen that the negative ε_{eff} appears at 8–14 GHz. The value of the ε_{eff} increases as the frequency increases. Hence, we can predict that the value of the refractive index is negative and increases to 0 as the frequency increases from 9.8 GHz to 12.5 GHz. The measured transmission spectra for permanent magnetic ferrite-based metamaterial is shown in Fig. 1c. One can see that there is a broad passband in the transmission spectra. It has been proved that the passband emerges just in the region where both permeability and permittivity are negative, which means that the metamaterials have negative refractive index. The passband appears at the frequency range from 10 to 12.2 GHz, which is in good agreement with the results shown in Fig. 1b. Due to using the different permanent magnetic ferrite to prepare metamaterials, the losses in the passband for the permanent magnetic ferrite-based metamaterials are higher than that for the photonic crystal in Ref. 29. In addition, the transmission property along *y* direction is the same as that along the *x* direction. In Ref. 29, the passband of the photonic crystal in Γ-M direction is different from that in Γ-K direction. In comparison with the photonic crystal, the permanent magnetic ferrite-based metamaterial shows a better consistency in transmission property.

Performance simulation for wedge-shaped structure. To corroborate the theoretical design, we have simulated the propagation of TE wave through a wedge using the retrieved effective material parameters at the working frequency $f = 10.85$ GHz. The magnitude of the incident power is 1 W. The wedge angle is 26.6° and the side lengths are 110 mm, 55 mm, and 120 mm, respectively. The distribution of electric field is shown in Fig. 2. The arrows represent the propagation direction of the wave. There is no refraction at the first surface due to the source wave of 10.85 GHz normally incident on the vertical surface of the wedge. The wave passes through the wedge and undergoes an obvious negative refraction at the second surface.

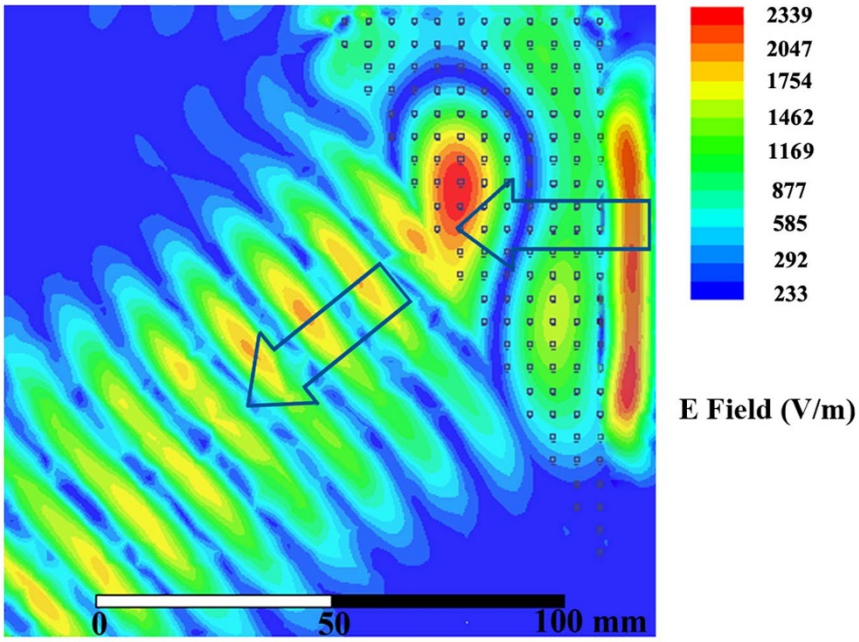

Figure 2 | Simulation of distribution of electric field for wedge-shaped sample. The incident wave is coming from the right, shooting normally onto the vertical surface of the wedge. The dots represent the wedge-shaped sample. The wedge angle is 26.6° and the side lengths are 110 mm, 55 mm, and 120 mm, respectively. Arrows represent the propagation direction of the wave.

Near-field scanning system. To confirm the simulated results of the negative refractive behavior of the permanent magnetic ferrite-based metamaterial, we have utilized the near-field scanning system (microwave planar waveguide)[31] to measure the propagation of an electromagnetic wave through the wedge composed of permanent magnetic ferrite rods and metallic wires. The photograph of the near-field scanning system is shown in Fig. 3a. The upper and lower metal plates form the planar waveguide, which restrict the polarization of the electric field to lie uniformly along the *z* direction and further restrict propagation to the *x*-*y* plane. A rectangular waveguide is utilized in the lower plate as the waveguide adapter to excite a plane wave (8–18 GHz). Only the electromagnetic wave with TE_{10} mode can propagate in this waveguide. The incident wave is formed by the creation of a channel in absorbing material and the wedge sample is placed directly at the end of the channel. A detecting probe is installed in the upper plate to measure the amplitude and phase of the local electric field. The feeding and detecting probes are connected to the output and input ports of the vector network analyzer (Agilent ENA5071C), respectively. The lower metal plate is carried by the 2D moving stage, which can be controlled by a computer to move in *x* and *y* directions with a scanning step of 4 mm so that we can measure electromagnetic field distributions within a certain area. A wedge-shaped sample was placed in the near-field scanning system. The wedge angle is 26.6° and the side lengths are 110 mm, 55 mm, and 120 mm, respectively. Besides, a slab-shaped sample has also been prepared, as shown in Fig. 3b. The slab is 150 mm long and 20 mm wide, with a point source placed 5 mm from the longer side of the slab.

Near-field scanning maps for wedge-shaped structure. The measured electric fields (real part and phase) for an incident wave at a series of frequencies refracting from a wedge are shown in Fig. 4. The wedge boundaries are shown by the dashed lines and the normal of the wedge surface is shown by the dotted line. The incident wave is

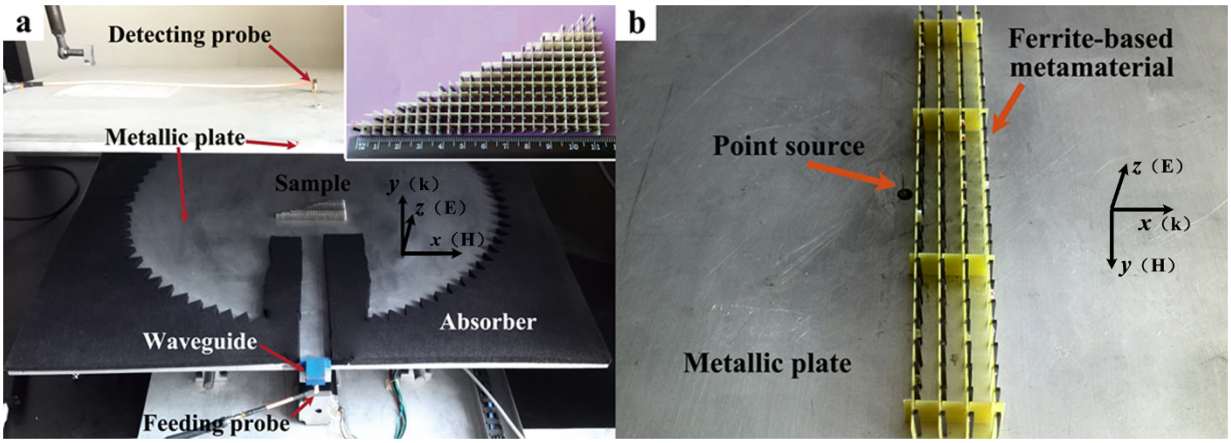

Figure 3 | Near-field scanning setup. (a) Photograph of the near-field scanning system. The inset shows the optical image of the as-prepared wedge sample composed of permanent magnetic ferrite rods and metallic wires. The wedge angle is 26.6° and the side lengths are 110 mm, 55 mm, and 120 mm, respectively. (b) Optical images of the as-prepared slab sample placed next to the point source in the near-field scanning system. The slab is 150 mm long and 20 mm wide, with a point source placed 5 mm from the longer side of the slab.

coming from the right, shooting normally onto the vertical surface of the wedge. Arrows represent the propagation direction of the wave. In order to demonstrate the negative refractive properties, we chose three frequencies of the wave, which is respectively 9.85 GHz (strong absorption), 10.85 GHz (negative refractive index), 15.8 GHz (far away from FMR). The electric field (real part) for the source wave at 9.85 GHz propagating into the wedge is shown in Fig. 4a. There is no wave appeared in the left area of the wedge. From Fig. 1b, the permeability of the permanent magnetic ferrite is negative at 9.85 GHz, but it is well known that there are large losses around the FMR frequency. In addition, the wedge-shaped sample has a large number of ferrite rods. Hence, the strong absorption leads to the above phenomenon. The waves at the upper and lower of the map are coming from the same source with no obstruction. Figure 4b shows the phase mapping for the source wave at 9.85 GHz propagating into the wedge, exhibiting the same result as that in Fig. 4a. When the source wave of 10.85 GHz is incident upon the wedge, the measured spatial maps of real part and phase of electric field are demonstrated in Fig. 4c and 4d. Due to the wave normally incident on the vertical surface of the wedge, there is no refraction at the first surface. The wave passes through the wedge and undergoes an obvious negative refraction at the second surface. The negative

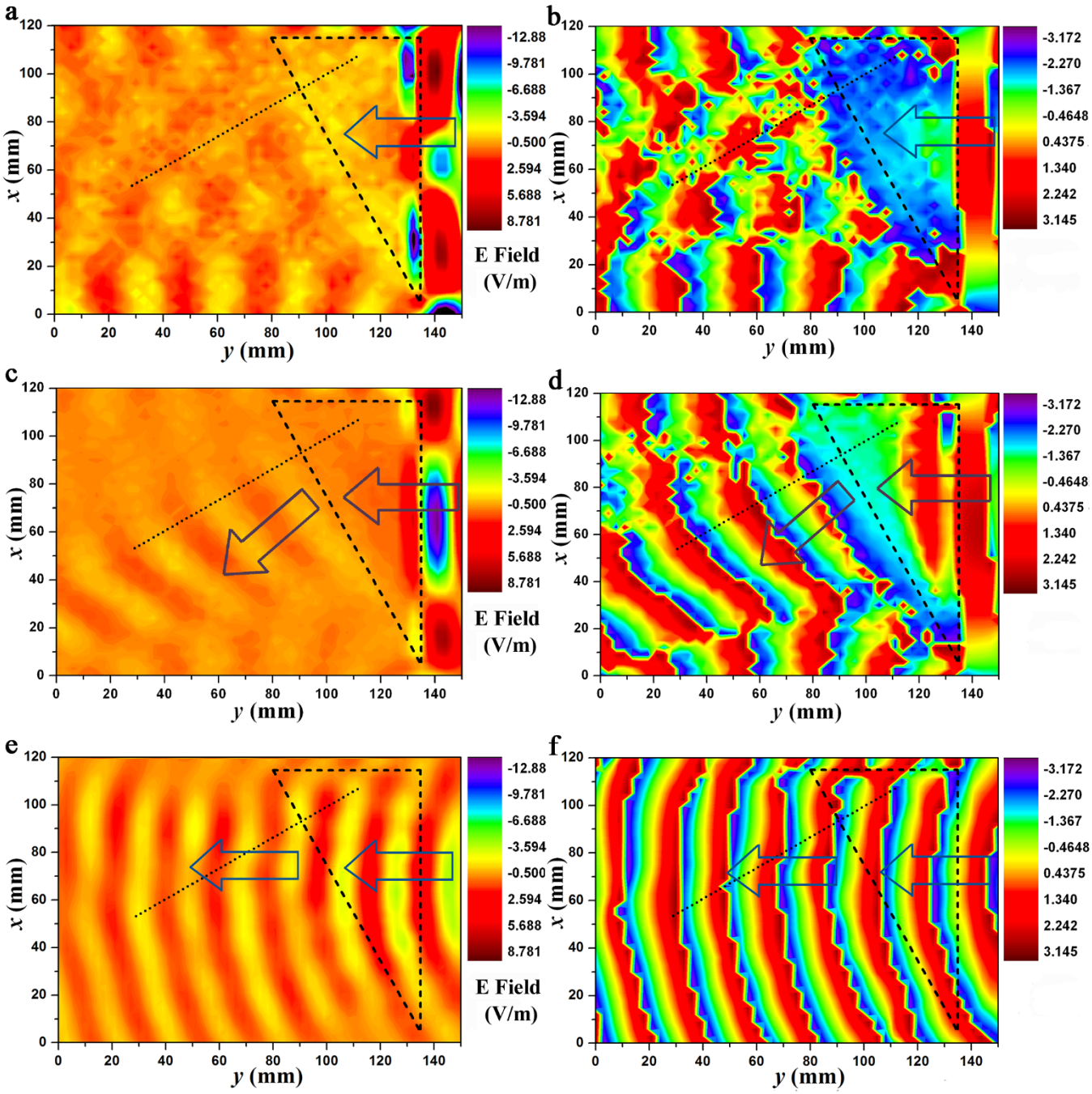

Figure 4 | Measured near-field scanning maps demonstrating the refractive properties. The measured spatial maps of (a) real part and (b) phase of electric field for an incident wave at 9.85 GHz (strong absorption), (c) real part and (d) phase of electric field for an incident wave at 10.85 GHz (negative refractive index), (e) real part and (f) phase of electric field for an incident wave at 15.8 GHz (far away from FMR) refracting from a wedge. The wedge boundaries are shown by the dashed lines and normal of the wedge surface is shown by the dotted line. The incident wave is coming from the right, shooting normally onto the vertical surface of the wedge. Arrows represent the propagation direction of the wave.

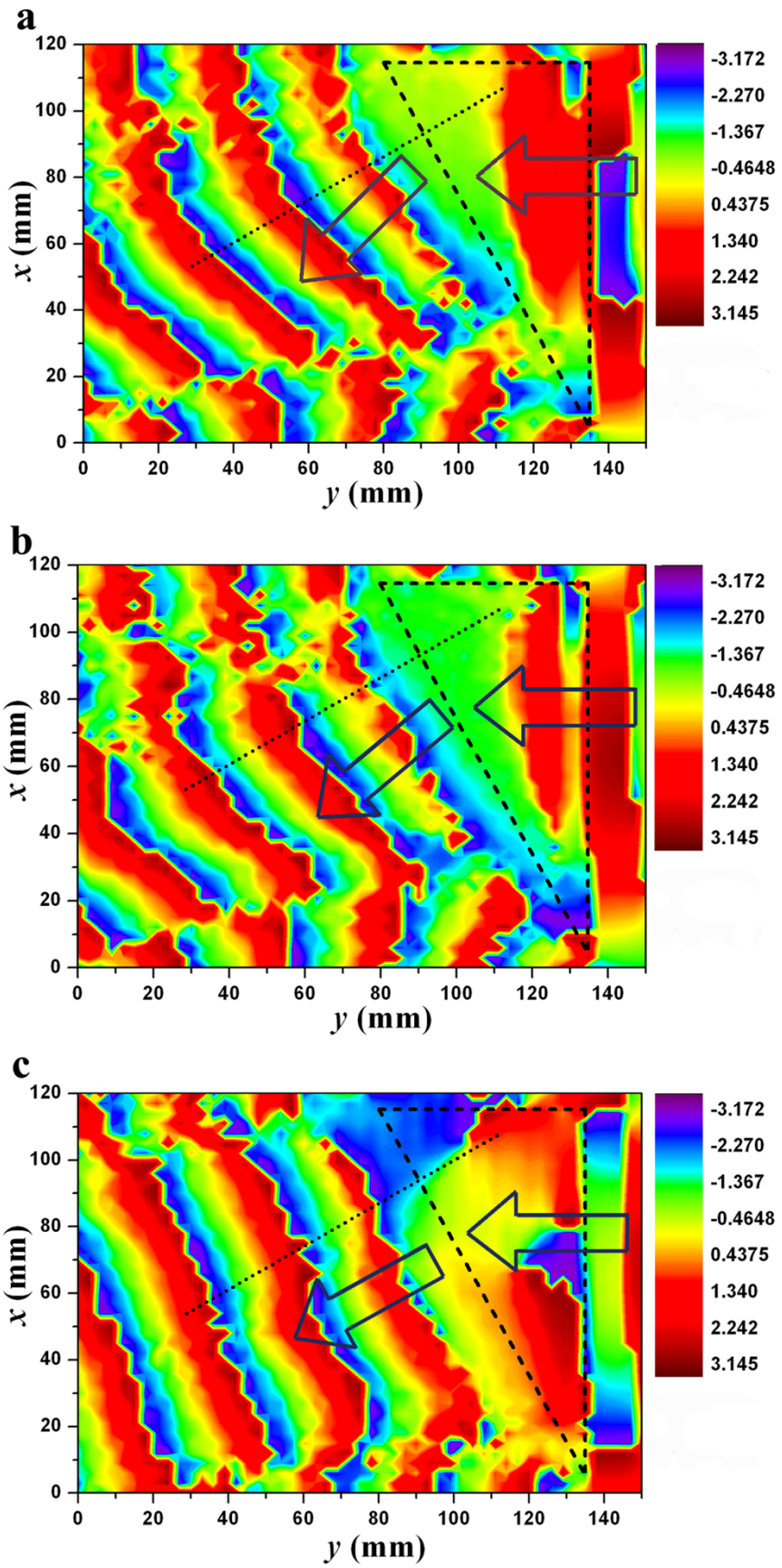

Figure 5 | Measured near-field scanning maps demonstrating the transition of the refractive behavior. The measured spatial maps of the phase of electric field for an incident wave at (a) 10.4 GHz (negative refractive index), (b) 11.5 GHz (negative refractive index), and (c) 12.2 GHz (near-zero refractive index) refracting from a wedge.

refractive behavior observed in the experimental results is in good agreement with that observed in simulated ones. When the frequency of the wave increases to 15.8 GHz which is far away from the FMR, the coupling between the ferrite and the electromagnetic field is weak. The wave does not interact with the ferrite strongly and the refractive index of the ferrite is close to 1[26]. Therefore, the wave passes through the wedge with the positive refraction, as shown in Fig. 4e and 4f.

Compared with the real part mapping of the electric field, the phase mapping can exhibit the refractive behavior more obviously. The measured spatial maps of the phase of electric field for an incident wave at a series of frequencies refracting from a wedge are shown in Fig. 5. In all cases, the propagation direction of the refracted wave lies on the same side of the surface normal as the incident wave. In Fig. 5a, one observes that the incident wave at 10.4 GHz has a certain refraction angle (about 18°) from the normal of the second surface. The phase mapping of the electric field for the source wave at 11.5 GHz propagating into the wedge is shown in Fig. 5b. In contrast to the incident wave at 10.4 GHz, the incident wave at 11.5 GHz has a relatively small refraction angle (about 10°) from the normal of the second surface. In Fig. 5c, when the frequency of the wave increases to 12.2 GHz, the wave has a near zero refraction angle from the normal, which exhibits a near zero refractive behavior. Based on the FMR behavior of the gyromagnetic ferrites, the effective permeability of the permanent magnetic ferrite rod is changing from negative to zero as the frequency of the wave increases. Since the index of refraction is directly related to the permeability via $n=\sqrt{\varepsilon\mu}$, the permanent magnetic ferrite-based metamaterials could exhibit near zero refractive index, which results in the near zero refractive behavior as shown in Fig. 5c.

Negative refractive behavior in slab-shaped structure. To further prove the negative refractive behavior of the permanent magnetic ferrite-based metamaterial, the simulated map of distribution of electric field at a frequency of 10.55 GHz for a slab placed next to a point source is shown in Fig. 6a. The material parameters used in this simulation are chosen to be consistent with the measured ones. The wave emanating from the point source located at the lower side of the slab is refocused to a point at the upper side of the slab. It looks like a point source existed at the upper side of the slab, and the electromagnetic wave continues emanating from this point. This behavior indicates the slab has a negative refractive index and the refractive index n approximately equal to -1. Besides simulation, a slab-shaped sample composed of permanent magnetic ferrite rods and metallic wires has also been prepared. The measured spatial map of the real part of electric field for a slab placed next to a point source at a frequency of 10.55 GHz is shown in Fig. 6b. The slab boundaries are shown by the dashed lines. The black dot represents the point source which is below the slab. It can be seen that the refractive behavior observed in experimental results is in good agreement with that observed in simulated ones. When the wave emanating from the point source passes through the slab, it is refocused to a point at the other side of the slab. The focusing behavior observed in simulation and experiment confirms the negative refractive properties of the permanent magnetic ferrite-based metamaterials.

Discussion

We fabricated a metamaterial composed of permanent magnetic ferrite rods and metallic wires. Due to high effective internal magnetic anisotropy, the permanent magnetic ferrite can provide effective negative permeability without external magnetic field when the nature resonance takes place. We prepared the wedge-shaped and slab-shaped structures of permanent magnetic ferrite-based metamaterials to investigate the refractive properties. Our design has been corroborated by the numerical calculation and measured near-field scanning electric field maps demonstrating that this metamaterial exhibits both negative refraction and near zero refraction. We believe that our results will pave the way for a new class of ferrite-based metamaterials without resorting to an external magnetic field bias. In contrast to the previous ferrite-based metamaterials, such a metamaterial has greater potential for practical applications such as waveguiding and imaging.

Methods

Theoretical description. The negative permeability of the ferrite can be obtained when the FMR takes place. The equation of the effective permeability for the soft magnetic ferrite under an applied magnetic field is well known from the ferromagnetic resonance (FMR) studies and can be expressed by[24]

$$\mu_{\mathrm{eff}}(\omega)=1-\frac{F\omega_{\mathrm{mp}}^2}{\omega^2-\omega_{\mathrm{mp}}^2-i\Gamma(\omega)\omega} \tag{1}$$

with

$$\Gamma(\omega)=\left(\frac{\omega^2}{\omega_{\mathrm{r}}+\omega_{\mathrm{m}}}+\omega_{\mathrm{r}}+\omega_{\mathrm{m}}\right)\alpha \tag{2}$$

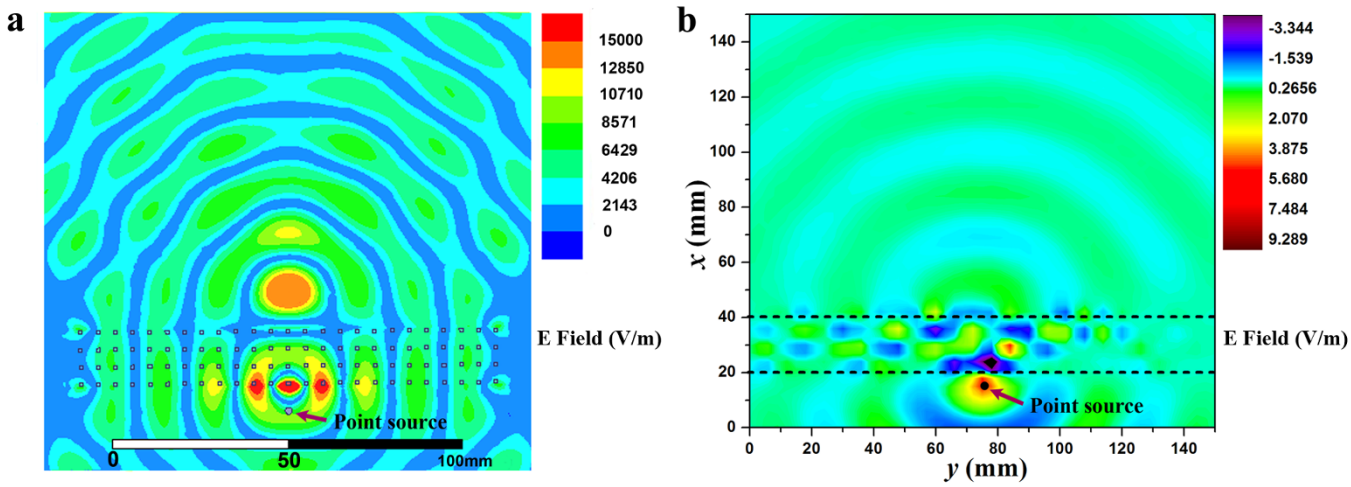

Figure 6 | Focusing maps demonstrating the negative refractive behavior. (a) Simulation of distribution of electric field and (b) measured spatial maps of the real part of electric field for a slab placed next to a point source at a frequency of 10.55 GHz. The slab boundaries are shown by the dashed lines. The black dot represents the point source which is below the slab.

$$\omega_{mp} = \sqrt{\omega_r(\omega_r + \omega_m)} \quad (3)$$

$$\omega_m = 4\pi M_s \gamma \quad (4)$$

$$\omega_r = \gamma\sqrt{[H_0 + H_a + (N_x - N_z)4\pi M_s][H_0 + H_a + (N_y - N_z)4\pi M_s]} \quad (5)$$

where α is damping coefficient of ferromagnetic precession, γ is the gyromagnetic ratio, $F = \omega_m/\omega_r$, ω_m and ω_r are characteristic frequency and FMR frequency of the ferrite, M_s is the saturation magnetization caused by the applied magnetic field, H_0 is the applied magnetic field, H_a is the magnetocrystalline anisotropy field, N_x, N_y, and N_z are the demagnetization factor for x, y, and z directions, respectively.

As is well known, the permanent magnetic ferrite possesses a giant magnetocrystalline anisotropy field. Hence, the permanent magnetic ferrite has a large remanent magnetization M_r at the easy magnetization direction after the magnetization process. By interacting with the magnetic field of an electromagnetic wave, the FMR can take place in the permanent magnetic ferrite without external magnetic field, which is called nature resonance. The characteristic frequency ω_m and FMR frequency ω_r of the permanent magnetic ferrite can be expressed as[32]

$$\omega_m = 4\pi M_r \gamma \quad (6)$$

$$\omega_r = \gamma\sqrt{[H_a + (N_x - N_z)4\pi M_r][H_a + (N_y - N_z)4\pi M_r]} \quad (7)$$

From Eq. (7), one can see that the FMR frequency of the permanent magnetic ferrite is determined by the anisotropy field and demagnetising field. Eqs. (1), (2), (3), (6) and (7) provide an insight into the physics about the effective permeability of the permanent magnetic ferrite. The negative permeability of the ferrite appears at an upper frequency region above the FMR frequency. Periodic continuous metallic wires can produce effective negative permittivity and ferrites provide effective negative permeability. By combining the ferrites and metallic wires, the negative refractive properties can be realized.

Sample fabrication. As a typical M-type hexagonal ferrites, $BaFe_{12}O_{19}$ presents permanent magnetic bias due to its high effective internal magnetic anisotropy. The commercial $BaFe_{12}O_{19}$ rods were sliced with dimensions of $1 \times 1 \times 10$ ($l \times w \times h$) mm^3. The height direction is along the easy magnetization direction. The saturation magnetization M_s, remanent magnetization M_r, linewidth ΔH and relative permittivity ε_r of the $BaFe_{12}O_{19}$ rods are 2800 Oe, 2000 Oe, 1200 Oe, and 16.4, respectively. The size of the copper wires is $0.5 \times 0.03 \times 10$ ($l \times w \times h$) mm^3. The permanent magnetic ferrite-based metamaterial is composed of $BaFe_{12}O_{19}$ rods and Cu wires. The optical image of the as-prepared wedge sample composed of $BaFe_{12}O_{19}$ rods and Cu wires is shown as an inset in Fig. 3a and the slab sample is shown in Fig. 3b. Using a shadow mask/etching technique, we prepared 0.4 mm thick FR-4 dielectric substrates ($\varepsilon_r = 4.4$ and $\tan\delta = 0.014$) with copper wires spacing of 5 mm on one side. The $BaFe_{12}O_{19}$ rods were pasted back-to-back with copper wires on the other side of the substrates. The permanent magnetic ferrite-based metamaterials were obtained by assembled the rod-wire units into a wedge-shaped structure or a slab-shaped structure. In order to measure the scattering parameters, a rectangular sample was also prepared, which has the same structure as shown in Ref. 24.

1. Veselago, V. G. The electrodynamics of substance simultaneously negative values of ε and μ. *Sov. Phys. Usp.* **10**, 509–514 (1968).
2. Pendry, J. B. Negative Refraction Makes a Perfect Lens. *Phys. Rev. Lett.* **85**, 3966–3969 (2000).
3. Schurig, D. *et al.* Metamaterial Electromagnetic Cloak at Microwave Frequencies. *Science* **314**, 977–980, 1133628 (2006).
4. Ramakrishna, S. A. Physics of negative refractive index materials. *Rep. Prog. Phys.* **68**, 449–521 (2005).
5. Ma, H. F. & Cui, T. J. Three-dimensional broadband and broad-angle transformation-optics lens. *Nat. Commun.* **1**, 124 (2010).
6. Liu, M. *et al.* Terahertz-field-induced insulator-to-metal transition in vanadium dioxide metamaterial. *Nature* **487**, 345–348 (2012).
7. Paul, T., Menzel, C., Rockstuhl, C. & Lederer, F. Advanced Optical Metamaterials. *Adv. Mater.* **22**, 2354–2357 (2010).
8. Chen, P.-Y., Farhat, M. & Alù, A. Bistable and Self-Tunable Negative-Index Metamaterial at Optical Frequencies. *Phys. Rev. Lett.* **106**, 105503 (2011).
9. Stefan, Linden *et al.* Magnetic Response of Metamaterials at 100 Terahertz. *Science* **306**, 1351–1353 (2004).
10. Ren, M., Plum, E., Xu, J. & Zheludev, N. I. Giant nonlinear optical activity in a plasmonic metamaterial. *Nat. Commun.* **3**, 833 (2012).
11. Fang, N. *et al.* Ultrasonic metamaterials with negative modulus. *Nat. Mater.* **5**, 452–456 (2006).
12. Lapine, M., Shadrivov, I. & Kivshar, Y. Wide-band negative permeability of nonlinear metamaterials. *Sci. Rep.* **2**, 412 (2012).
13. Bouillard, J.-S., Vilain, S., Dickson, W., Wurtz, G. A. & Zayats, A. V. Broadband and broadangle SPP antennas based on plasmonic crystalswith linear chirp. *Sci. Rep.* **2**, 829 (2012).
14. Maslovski, S. I., Tretyakov, S. A. & Belov, P. A. Wire media with negative effective permittivity: A quasi-static model. *Microwave Opt. Technol. Lett.* **35**, 47–51 (2002).
15. Magnus, F. *et al.* A d.c. magnetic metamaterial. *Nat. Mater.* **7**, 295–297 (2008).
16. Katsarakis, N. *et al.* Left- and right-handed transmission peaks near the magnetic resonance frequency in composite metamaterials. *Phys. Rev. B* **70**, 201101 (2004).
17. Zhou, J. *et al.* Saturation of the Magnetic Response of Split-Ring Resonators at Optical Frequencies. *Phys. Rev. Lett.* **95**, 223902 (2005).
18. Dewar, G. A thin wire array and magnetic host structure with n<0. *J. Appl. Phys.* **97**, 10Q101 (2005).
19. Dewar, G. Minimization of losses in a structure having a negative index of refraction. *New J. Phys.* **7**, 161–161 (2005).
20. Poo, Y. *et al.* Experimental verification of a tunable left-handed material by bias magnetic fields. *Appl. Phys. Lett.* **96**, 161902 (2010).
21. Rachford, F., Armstead, D., Harris, V. & Vittoria, C. Simulations of Ferrite-Dielectric-Wire Composite Negative Index Materials. *Phys. Rev. Lett.* **99**, 057202 (2007).
22. Huang, Y. J., Wen, G. J., Yang, Y. J. & Xie, K. Tunable dual-band ferrite-based metamaterials with dual negative refractions. *Appl. Phys. A* **106**, 79–86 (2011).
23. He, P. *et al.* Q-band tunable negative refractive index metamaterial using Sc-doped BaM hexaferrite. *J. Phys. D: Appl. Phys.* **42**, 155005 (2009).
24. Zhao, H., Zhou, J., Kang, L. & Zhao, Q. Tunable two-dimensional left-handed material consisting of ferrite rods and metallic wires. *Opt. Express* **17**, 13373–13380 (2009).
25. Bi, K., Zhou, J., Zhao, H., Liu, X. & Lan, C. Tunable dual-band negative refractive index in ferrite-based metamaterials. *Opt. Express* **21**, 10746 (2013).
26. Liu, S. *et al.* Manipulating Negative-Refractive Behavior with a Magnetic Field. *Phys. Rev. Lett.* **101**, 157407 (2008).
27. Shalaby, M., Peccianti, M., Ozturk, Y. & Morandotti, R. A magnetic non-reciprocal isolator for broadband terahertz operation. *Nat. Commun.* **4**, 1558 (2013).
28. Harris, V. G. *et al.* Recent advances in processing and applications of microwave ferrites. *J. Magn. Magn. Mater.* **321**, 2035–2047 (2009).
29. Gu, Y. *et al.* Self-biased magnetic left-handed material. *Appl. Phys. Lett.* **102**, 231914 (2013).
30. Smith, D. R. Analytic expressions for the constitutive parameters of magnetoelectric metamaterials. *Phys Rev E* **81**, 036605 (2010).
31. Justice, B. J. *et al.* Spatial mapping of the internal and external electromagnetic fields of negative index metamaterials. *Opt. Express* **14**, 8694–8705 (2006).
32. Kong, L. B. *et al.* Recent progress in some composite materials and structures for specific electromagnetic applications. *Int. Mater. Rev.* **58**, 203–259 (2013).

Acknowledgments

This work was supported by the National High Technology Research and Development Program of China under Grant No. 2012AA030403, the National Natural Science Foundation of China under Grant Nos. 51032003, 11274198, 51102148 and 51221291, the Shandong Natural Science Foundation under Grant No. ZR2010AM025, and the China Postdoctoral Research Foundation under Grant No. 2013M530042.

Author contributions

K.B. and J.Z. conceived the idea and designed experiments. K.B., Z.Q.X., C.W.L. and Q.Z. performed the experiments. K.B., C.W.L., X.M.L., G.Y.D. and H.J. Z. developed the post-processing treatments of the experimental data. K.B. and Y.S.G. carried out numerical calculations and figures. K.B. and J.Z. wrote the paper. All authors contributed to scientific discussion and critical revision of the article.

Additional information

Competing financial interests: The authors declare no competing financial interests.

How to cite this article: Bi, K. *et al.* Negative and near zero refraction metamaterials based on permanent magnetic ferrites. *Sci. Rep.* **4**, 4139; DOI:10.1038/srep04139 (2014).